A tri-phasic continuum model for the numerical analysis of biological tissue proliferation using the Theory of Porous Media.

Application to cardiac remodelling in rheumatic heart disease

Adam Mosam[1,2,*], *Sebastian* Skatulla[1,2], and *Ntobeko* Ntusi[3]

[1]Computational Continuum Mechanics Group, Department of Civil Engineering, University of Cape Town,South Africa

[2]Centre for Research in Computational and Applied Mechanics, University of Cape Town, South Africa

[3]Division of Cardiology, Department of Medicine, University of Cape Town, South Africa

Abstract. This research is part of an on-going project aimed at describing the mechanotransduction of rheumatic heart disease (RHD), in order to study long-term effects of new therapeutic concepts to treat inflammatory heart diseases and ultimately, estimate their effectiveness to prevent heart failure. RHD is a condition which is mostly common amongst low-income countries and accounts for approximately 250 000 deaths per annum. The Theory of Porous Media (TPM) can represent the proliferative growth and remodelling processes related to RHD within a thermodynamically consistent framework and is additionally advantageous with application to biological tissue due to the ability to couple multiple constituents.

The research presented will extend an existing biphasic TPM model for the solid cardiac tissue (solid phase) saturated in a blood and interstitial fluid (liquid phase) [1], to a triphasic model with the inclusion of a third nutrient phase towards growth. This inclusion is motivated by the reason to constrain the volume of the liquid phase within the system in response to the description of growth, which is modelled through a mass exchange between the solid phase and liquid phase within the biphasic model. Although the nutrient phase acts as a source for growth, the proposed mass supply function used to correlate the deposition of sarcomeres in relation to growth is predominantly mechanically driven and bears no connection to any biochemical constituent, which therefore renders the nutrient phase as a physiologically arbitrary quantity. However, the provision of the nutrient phase is a platform for the inclusion of known constituents which actively contribute towards growth, which may be explored in future research.

The triphasic model is applied to a full cardiac cycle of a left ventricle model, extracted from cardiovascular magnetic resonance (CMR) scans of patients diagnosed with RHD.

*e-mail: msmada002@myuct.ac.za

1 Introduction

1.1 Cardiovascular disease

Cardiovascular disease is the most prevalent cause of death globally, accounting 40% of all human mortality [2]. Even through significant medical advancement, approximately 25 million people suffer from heart failure, annually [3]. Unlike other types of tissue in the body, cardiac tissue is unique in the sense that it can rarely regenerate after being damaged [4].

Attention will be given to rheumatic heart disease (RHD), a chronic heart condition which is caused by a series of attacks of *rheumatic fever* [5]. Valvular dysfunction is the critical feature of RHD whereby the valves of the left ventricle are most commonly left in a state of permanent damage or complete failure [5, 6]. Hypertrophy of the muscle walls of the left ventricle is induced as a result of valvular dysfunction [6, 7]. Hypertrophy of the ventricle may either be in the form of concentric or eccentric growth, whereby cardiomyocytes are added in parallel (increase in thickness) or in series (elongation of the tissue), respectively [8]. Within this study, attention will be focused on the case of eccentric hypertrophy in relation to left ventricle dilation (LVD).

1.2 Biological and cardiac modelling

Cardiac modelling is viewed as the benchmark for soft tissue modelling, with much attention given to growth in arteries, with respect to cardiovascular disease [9, 10], and full scale heart modelling [11–14]. The characterisation of cardiac tissue growth in relation to biochemical stimulants, is not well understood. Hence, the studies which model growth proliferation are mechanically driven. A common example is found in the growth laws formulated to model eccentric and concentric hypertrophy through stress and strain based laws, respectively, proposed by Goktepe et al. [11]. Growth related modelling of cardiac tissue generally makes use of transversely isotropic growth laws, due to the composition of the muscle structure[12]. In the work of Werner et al. [15], transversely isotropic and isotropic growth was initiated on circular discs, defined as cardiac tissue material. This study employed a theory of porous media framework. The Theory of Porous Media (TPM) is advantageous in terms of soft tissue modelling as it is able to capture solid-fluid interaction [16]. In addition to the aforementioned citation, TPM has been utilised in describing soft tissue and multiphase systems in recent times, such as with the study of the liver in the work of Ricken et al. [16], and with a patient-specific left ventricle, conducted by Hopkins [1].

This research entails adding a third phase to an existing biphasic TPM framework, implemented in an in-house computational mechanics software SESKA. The biphasic constituents comprise of a solid and fluid phase, which poses a few problems in relation to growth proliferation [1]. Mitigating these problems associated with the biphasic model could be realised by creating a triphasic model through introduction of a third nutrient phase [1]. In this research, the triphasic model proposed is based on a model developed by Ricken et al. [17].

In terms of growth, a more efficient, and mathematically consistent method of expressing the growth evolution, which is derived from the balance equation of mass and represented through the growth Jacobian, is available in the work of Werner [18], as compared to that implemented in the current biphasic model. Coupling this growth evolution method with a strain driven, transversely isotropic growth law, for the case of LVD, will hence form the second major objective of this research.

2 Triphasic material model

In the framework of TPM, a solid porous skeleton is saturated with pore fluids, which constitute the κ constituents of the control space. The control space, at time t, is defined by B_S and

bordered by the surface ∂B_S. The *volume fraction* n^α, may be defined as the local volume portion which belongs to the individual constituents φ^α, and relates the constituent volume elements dv^α to the bulk volume elements dv, by

$$n^\alpha(\mathbf{x}, t) = \frac{dv^\alpha}{dv}, \qquad \sum_{\alpha}^{S,L,N} n^\alpha(\mathbf{x}, t) = \sum_{\alpha}^{S,L,N} \frac{\rho^\alpha}{\rho^{\alpha R}} = 1 \tag{1}$$

with α being one of the κ constituents. For the triphasic model used in this research, solid, liquid and nutrient constituents are used, such that $\alpha \in \{S, L, N\}$. Furthermore, $\mathbf{x}$ is the spatial position at time t and ρ^α is the partial density, which relates to the real density $\rho^{\alpha R}$, by $\rho^\alpha = n^\alpha \rho^{\alpha R}$. Eq.$(1)_2$ describes what is termed the *saturation condition*, and should always be fulfilled.

2.1 Kinematics

The saturated porous solid will be idealized as a statistically distributed immiscible mixture comprising of constituents φ^α with particles $\mathbf{X}_\alpha$, that have independent motion functions $\mathbf{x} = \chi_\alpha(\mathbf{X}_\alpha, t)$. This represents the *Lagrange* description of motion. With χ_α being unique and continuous, its inverse mapping leads to the *Eulerian* description of motion $\mathbf{X}_\alpha = \chi_\alpha^{-1}(\mathbf{x}, t)$. This statement may only be true if the mathematical condition of a non-zero *Jacobian* $J_\alpha = \det\mathbf{F}_\alpha \neq 0$, is satisfied for each constituent, with $\mathbf{F}_\alpha$ being the *deformation gradient* $\mathbf{F}_\alpha = \frac{\partial \chi_\alpha}{\partial \mathbf{X}_\alpha}$. Each constituent possesses its own velocity and acceleration field. In the Lagrangian configuration, these are stated as

$$\mathbf{x}'_\alpha = \frac{\partial \chi_\alpha(\mathbf{X}_\alpha, t)}{\partial t}, \qquad \mathbf{x}''_\alpha = \frac{\partial^2 \chi_\alpha(\mathbf{X}_\alpha, t)}{\partial t^2} \tag{2}$$

In the Eulerian configuration, the motion of a particle is governed by time t, and the spatial position $\mathbf{x}$. For an arbitrary scalar-value function $\Gamma(\mathbf{x}, t)$, the *material time derivative* is defined as $(\Gamma)'_\alpha = \frac{\partial \Gamma}{\partial t} + \mathrm{grad}\Gamma \cdot \mathbf{x}'_\alpha$, where "grad$(\cdot)$" denotes the partial derivative of $(\cdot)$ with respect to the spatial position. Similarly, Grad$(\cdot)$ is defined as the partial derivative with respect to the material position.

For problems involving a multiphase coupling of a porous solid and $\kappa - 1$ fluids, one would generally continue from a Lagrangian description of the solid phase, with the solid displacement vector $\mathbf{u}_S$, being the unknown variable, determined by $\mathbf{u}_S = \mathbf{x} - \mathbf{X}_S$. However, with respect to the fluid phases, greater ease is found by adopting the Eulerian setting and by using the relative velocity between each respective fluid phase and the solid skeleton [19]. Consequently the *seepage velocity* is introduced as $\mathbf{w}_{\beta S} = \mathbf{x}'_\beta - \mathbf{x}'_S$.

The *spatial velocity gradient* is given by $\mathbf{L}_\alpha = \frac{\partial \mathbf{x}'_\alpha}{\partial \mathbf{x}}$, or alternatively as $\mathbf{L}_\alpha = (\mathbf{F}_\alpha)'_\alpha \mathbf{F}^{-1}{}_\alpha$. The spatial velocity gradient may be decomposed into its symmetric part $\mathbf{D}_\alpha = \frac{1}{2}\left(\mathbf{L}_\alpha + \mathbf{L}_\alpha^T\right)$, and skew-symmetric part $\mathbf{W}_\alpha = \frac{1}{2}\left(\mathbf{L}_\alpha - \mathbf{L}_\alpha^T\right)$.

2.2 Kinematics of Growth

The kinematic approach used employs a multiplicatively split deformation gradient $\mathbf{F}_S$ into an elastic part $\mathbf{F}_{Se}$, and a growth part $\mathbf{F}_{Sg}$, such that $\mathbf{F}_S = \mathbf{F}_{Se}\mathbf{F}_{Sg}$ [20]. This results in the formation of a stress free intermediate configuration, whereby the deformation resulting parts are captured within the elastic zone (between the intermediate and actual configuration).

Following the description of the multiplicative decomposition of $\mathbf{F}_S$, the same principle may be applied to the Jacobian $J_S = J_{Se}J_{Sg}$, whereby it's comprised of an elastic part J_{Se},

which translates into volume change due to deformation, and an irreversible growth part J_{Sg}, which causes a volume change due to deposited matter. [21]

With $\mathbf{n}_0$ being the unit normal to the surface in the reference configuration, the total stretch ϵ in the actual configuration, in the direction of $\mathbf{n}_0$, is given by

$$\epsilon = \|\mathbf{F}_S\, \mathbf{n}_0\| = \epsilon_e \epsilon_g \tag{3}$$

where ϵ_e and ϵ_g represent the stretch components, in similar analogy to the previous quantities. With respect to cardiac tissue growth, ϵ_g would hence represent the stretch caused by a generation of sarcomeres in relation to a maladaptive response to a pressure or volume overload [11]. It should be noted that, ϵ_g may be taken to be equivalent to J_{Sg}. Finally, for transversely isotropic growth, the following expression is used to determine the growth part of the deformation gradient

$$\mathbf{F}_{Sg} = \mathbf{I} + (\epsilon_g - 1)\mathbf{n}_0 \otimes \mathbf{n}_0 \tag{4}$$

2.3 Balance equations

The balance equations of the constituents φ^α are analogous to those found in mixture theory [16]. The balance equations for a porous body may be given in terms of the balance of mass, momentum and the moment of momentum

$$(\rho^\alpha)'_\alpha + \rho^\alpha \mathrm{div}(\mathbf{x}'_\alpha) = \hat{\rho}^\alpha\,, \quad \mathrm{div}\mathbf{T}^\alpha + \rho^\alpha(\mathbf{b}^\alpha - \mathbf{x}''_\alpha) = \hat{\rho}^\alpha \mathbf{x}'_\alpha - \hat{\mathbf{p}}^\alpha\,, \quad \mathbf{T}^\alpha = (\mathbf{T}^\alpha)^T \tag{5}$$

respectively, where "div" denotes the spatial divergence operator, $\mathbf{T}^\alpha$ is the Cauchy stress tensor, and $\rho^\alpha \mathbf{b}^\alpha$ is the volume force. The source terms, $\hat{\rho}^\alpha$ and $\hat{\mathbf{p}}^\alpha$, represent the mass supply and interaction forces of momentum between the constituents φ^α, respectively.

2.4 Assumptions

For the case of the left ventricle comprising of a porous solid skeleton saturated with blood, material incompressibility may be assumed for the entire system, such that $\left(\rho^{\alpha R}\right)'_\alpha = 0$. The mass supply function for the nutrient phase $\hat{\rho}^N$ accounts for the increase in mass of the solid phase and an equivalent reduction in mass of the nutrient phase, which leads to $\hat{\rho}^N = -\hat{\rho}^S$. The motion function of the nutrient phase $\chi_N(\mathbf{X}_N, t)$ is taken to be equivalent to that of the liquid phase $\chi_L(\mathbf{X}_L, t)$. As a result, the motion functions of the liquid and nutrient phases will hence be represented in terms of a general fluid phase $\chi_F(\mathbf{X}_F, t)$. In addition, all body forces will be neglected and a quasi-static approach will be adopted, which results in all acceleration terms for the phases to be ignored $\mathbf{x}''_\alpha = \mathbf{0}$. Furthermore, the mass exchange term which contributes to momentum will be neglected due to the insignificant amount of momentum generated from the exchange of mass between the phases $\hat{\rho}^\alpha \mathbf{x}'_\alpha = \mathbf{0}$. The temperature difference between all the phases will be treated as negligible, as it is assumed that there is no differential temperature within the saturated tissue matrix.

2.5 Field equations

Considering the assumptions and restriction of mass supply terms, the balance of mass and momentum may be adapted to form the field equations required to model the proliferative process of growth and remodelling of cardiac tissue. Starting with the balance equation of mass, the local form may be rewritten in the form shown below for each constituent

$$\left(n^S\right)'_S + n^S \mathbf{D}_S : \mathbf{I} = \frac{\hat{\rho}^S}{\rho^{SR}}, \quad \left(n^L\right)'_L + n^L \mathbf{D}_L : \mathbf{I} = 0 \quad \left(n^N\right)'_N + n^N \mathbf{D}_N : \mathbf{I} = \frac{\hat{\rho}^N}{\rho^{NR}}, \tag{6}$$

such that the mass supply term for the liquid phase is neglected. The adapted forms of the balance equations of momentum for the mixture and for each constituent yields

$$\mathrm{div}\mathbf{T} = \mathbf{0}, \quad \mathrm{div}\mathbf{T}^{\mathrm{S}} + \hat{\mathbf{p}}^{\mathrm{S}} = \mathbf{0}, \quad \mathrm{div}\mathbf{T}^{\mathrm{L}} + \hat{\mathbf{p}}^{\mathrm{L}} = \mathbf{0}, \quad \mathrm{div}\mathbf{T}^{\mathrm{N}} + \hat{\mathbf{p}}^{\mathrm{N}} = \mathbf{0} \tag{7}$$

whereby the sum of the interaction forces $\hat{\mathbf{p}}^{\alpha}$, is zero and the quantity $\mathbf{T}$, represents the sum of the Cauchy stress tensor's of each constituent.

3 Constitutive modelling

Unlike the theory of mixtures, which is a closed framework that has an equivalent amount of unknowns and field equations, the theory of porous media differs in that it is constrained by the saturation condition, which stems from the volume fractions concept. This results in an additional field equation. Therefore, an additional scalar quantity needs to be introduced in the form of a *Lagrange multiplier* λ[16].

The Lagrange multiplier is introduced as a quantity by means of the entropy inequality, through the material time derivative of the saturation condition, shown in Eq.(1), and the adapted forms of the balance equations of mass Eq.(6). After evaluation of the entropy inequality (see [16]), expressions for the Cauchy stress tensor $\mathbf{T}^{\alpha}$ are yielded as

$$\mathbf{T}^{\mathrm{S}} = 2\rho^{\mathrm{S}}\mathbf{F}_{\mathrm{S}}\frac{\partial\psi^{\mathrm{S}}}{\partial\mathbf{C}_{\mathrm{S}}}\mathbf{F}_{\mathrm{S}}^{\mathrm{T}} - \lambda\mathrm{n}^{\mathrm{S}}\mathbf{I}, \quad \mathbf{T}^{\mathrm{F}} = \mathrm{n}^{\mathrm{F}}\lambda\mathbf{I}, \quad \mathrm{n}^{\mathrm{F}} = \mathrm{n}^{\mathrm{L}} + \mathrm{n}^{\mathrm{N}} \tag{8}$$

where the influence of the free Helmholtz free energy function of the fluid phases on the stress is neglected [16]. The following condition should be applied to the interaction force of the lumped fluid phase $\mathbf{p}^{\mathrm{F}}$ and the solid mass supply function $\hat{\rho}^{\mathrm{S}}$, in order to result in a valid entropy inequality:

$$\hat{\mathbf{p}}^{\mathrm{F}} = \lambda\mathrm{grad}\,\mathrm{n}^{\mathrm{F}} - \mathbf{S}^{\mathrm{F}}\mathbf{w}_{\mathrm{FS}}, \quad \hat{\rho}^{\mathrm{S}} = \delta(\Psi^{\mathrm{N}} - \Psi^{\mathrm{S}}) \tag{9}$$

where Ψ^{α} is the chemical potential of the constituents φ^{α}, and $\mathbf{S}^{\mathrm{F}}$ is a positive definite tensor which dictates the direction of fluid flow. The scaling parameter δ needs to be greater than or equal to zero in order to fulfil the entropy inequality conditions [16]. These expressions will be elaborated on in more detail in the following sections.

3.1 Stress

When the mitral valve reopens at the onset of the diastolic filling stage, blood is allowed to enter the ventricular cavity. It is assumed that, during this phase, the left ventricle does not exert any force but rather deforms and behaves in a passive manner. This results in a passive strain energy response, and may be represented using a strain energy function ψ^{S}. The last three phases of the cardiac cycle, namely; the isovolumetric contraction, ejection and isovolumetric relaxation, is termed the *active contraction* stage, and usually results in the muscle fibres contracting, which as a result causes the ventricular pressure within the cavity to increase due to the accumulated strain energy developed [7]. The total stress may hence be expressed as a superposition of the passive and active stresses

$$\mathbf{S} = \mathbf{S}_{\mathrm{P}} + \mathbf{S}_{\mathrm{A}} \tag{10}$$

where $\mathbf{S}_{\mathrm{P}}$ is the passive stress and $\mathbf{S}_{\mathrm{A}}$ is the active stress. $\mathbf{S}$ is related to the Cauchy stress tensor by $\mathbf{S} = \mathbf{F}_{\mathrm{S}}^{-1}\mathbf{T}\mathbf{F}_{\mathrm{S}}^{-\mathrm{T}}$, where $\mathbf{T} = \mathbf{T}^{\mathrm{S}} + \mathbf{T}^{\mathrm{F}}$. A more descriptive overview of the constitutive formulation used to represent the passive and active material behaviour, and the subsequent integration with a TPM framework, may be viewed in the works of Mosam [22] and Hopkins [1].

3.2 Seepage velocity

From Eq.(9), a constitutive law for the seepage velocity $\mathrm{n}^{\mathrm{F}}\mathbf{w}_{\mathrm{FS}}$ is proposed, for transversely isotropic flow [16]

$$\mathrm{n}^{\mathrm{F}}\mathbf{w}_{\mathrm{FS}} = \frac{\left(\mathrm{n}^{\mathrm{F}}\right)^2}{\alpha_{\mathrm{F0}}}\mathbf{M}\,\mathrm{grad}\,\lambda \tag{11}$$

which is dependent on the spatial change in pore pressure and the permeability of the system (controlled by the first term in Eq.(11)). The direction of the flow is governed by the structural tensor $\mathbf{M}$. In order to characterize the parameter α_{F0} the following relationships which involve either, the initial Darcy permeability $\mathrm{k}^{\mathrm{F}}_{0\mathrm{S}}(\mathrm{m/s})$ and the specific weight $\gamma^{\mathrm{FR}}(\mathrm{N/m^3})$ or the intrinsic solid permeability $\mathrm{k}^{\mathrm{F}}_{0\mathrm{S}}(\mathrm{m^2})$ and the effective shear viscosity $\mu^{\mathrm{FR}}(\mathrm{Ns/m^2})$, may be applied such that

$$\frac{\left(\mathrm{n}^{\mathrm{F}}\right)^2}{\alpha_{\mathrm{F0}}} = \left(\frac{\mathrm{n}^{\mathrm{F}}}{1\text{-}\mathrm{n}^{\mathrm{S}}_{0\mathrm{S}}}\right)^m \frac{\mathrm{k}^{\mathrm{F}}_{0\mathrm{S}}}{\gamma^{\mathrm{FR}}} = \left(\frac{\mathrm{n}^{\mathrm{F}}}{1\text{-}\mathrm{n}^{\mathrm{S}}_{0\mathrm{S}}}\right)^m \frac{\mathrm{k}^{\mathrm{F}}_{0\mathrm{S}}}{\mu^{\mathrm{FR}}} \tag{12}$$

where m is a dimensionless constant, see also Eipper [23], Ricken [16], Ehlers et al. [24] and the citations therein.

3.3 Mass supply

The proposed method of representing growth proliferation in cardiac tissue is based on that presented in the work of Werner [18]. This growth evolution model will hence be combined with a strain driven growth law, developed by Goktepe et al. [11], in order to model a dilated left ventricle. Making use of the balance equation of mass for the solid phase, the Jacobian may be expressed in its decomposed form

$$\mathrm{J}_{\mathrm{S}} = \underbrace{\frac{\rho^{\mathrm{S}}_{0\mathrm{S}}}{\rho^{\mathrm{S}}}}_{\mathrm{J}_{\mathrm{Se}}} \underbrace{\exp\left(\int \frac{\hat{\rho}^{\mathrm{S}}}{\rho^{\mathrm{S}}}\mathrm{d}t\right)}_{\mathrm{J}_{\mathrm{Sg}}} \tag{13}$$

comprised of the elastic part J_{Se}, and growth part J_{Sg}, see Sec.(2.2). Using a finite difference approximation, and by discretising the equation above with respect to the n^{th} and $(n+1)$ time step

$$\mathrm{J}^{n+1}_{\mathrm{Sg}} = \underbrace{\exp\left[\sum_{n=1}^{n}\left(\frac{\hat{\rho}^{\mathrm{S}}}{\rho^{\mathrm{S}}}\right)^n \Delta t^n\right]}_{\mathrm{J}^{n}_{\mathrm{Sg}}} \cdot \underbrace{\exp\left[\left(\frac{\hat{\rho}^{\mathrm{S}}}{\rho^{\mathrm{S}}}\right)^{n+1} \Delta t^{n+1}\right]}_{\Delta\mathrm{J}^{n+1}_{\mathrm{Sg}}} \tag{14}$$

results in a form where J_{Sg} may be updated every iteration. The mass supply function $\hat{\rho}^{\mathrm{S}}$ is postulated by

$$\hat{\rho}^{\mathrm{S}} = \hat{\rho}^{\max}\hat{\rho}^{\lim}, \quad \hat{\rho}^{\lim} = \begin{cases} \left(\frac{\mathrm{J}^{\max}_{\mathrm{Sg}} - \mathrm{J}_{\mathrm{Sg}}}{\mathrm{J}^{\max}_{\mathrm{Sg}} - 1}\right)^{\gamma} (\epsilon_{\mathrm{e}} - \epsilon_{\max}) & \text{if } \mathrm{J}_{\mathrm{Sg}} < \mathrm{J}^{\max}_{\mathrm{Sg}} \;\;\&\;\; \epsilon_{\mathrm{e}} > \epsilon_{\max} \\ 0 & \text{if } \mathrm{J}_{\mathrm{Sg}} \geq \mathrm{J}^{\max}_{\mathrm{Sg}} \;\text{ or }\; \epsilon_{\mathrm{e}} \leq \epsilon_{\max} \end{cases} \tag{15}$$

making use of a strain driven growth law [11]. $\hat{\rho}^{max}\,(\mathrm{kg/(s\,m^3)})$ denotes the maximum mass exchange rate. $\mathrm{J}^{\max}_{\mathrm{Sg}}$ represents the maximum growth factor, which acts to limit the amount of growth as J_{Sg} tends towards it, which is additionally controlled by the parameter γ.

4 Numerical treatment

Considering the set of unknown quantities for the triphasic model, shown by Eq.(16)

$$\mathcal{U} = \left\{ \mathbf{u}_{\mathrm{S}},\ \mathrm{n}^{\mathrm{S}},\ \mathrm{n}^{\mathrm{N}}, \lambda \right\} \tag{16}$$

the governing equations may be solved in order to quantify these variables. The displacement $\mathbf{u}_{\mathrm{S}}$ will be solved using the balance equation of momentum. The pore pressure λ will be calculated through the balance equation of mass of the mixture. Lastly, the solid and nutrient volume fractions n^{S} and n^{N}, will be determined using the respective balance equations of mass. Using the Galerkin approach, which transforms a system of equations into a discrete problem, allows the weak forms to be generated from the aforementioned balance equations.

The finite element method (FEM) is used as a numerical framework to approximate the differential equations present within the triphasic TPM model. The *Newton-Raphson* method is used to solve the system of non-linear equations, and the *Newmark-β* method is used as a temporal discretization scheme. These are implemented in the in-house software SESKA.

5 Numerical example using an RHD affected heart

The previous sections have established the mathematical framework needed for a triphasic TPM model, and additionally with application to cardiac systems which include growth and remodelling proliferation. This section will continue with an analysis of a patient specific heart, diagnosed with RHD. Investigation into the behavioural changes of the left ventricle will be conducted and will be furthermore used to validate the adequacy of the proposed TPM model.

The patient under study was diagnosed with RHD in 2014 after CMR (cardiovascular magnetic resonance) scanning, at the Groote Schuur Hospital. From the assessment, it was found that the patient had a severely stenosed mitral valve with moderate regurgitation. The patient was admitted for a valve replacement in 2015 whereby subsequent follow-up scans were taken in 2016. This investigation will involve the two scans taken in 2014 and 2016, which were modelled by Hopkins [1].

5.1 Applied boundary conditions

In order to build the boundary value problem needed for the geometry of the left ventricle, *Dirichlet* and *Neumann* boundary conditions need to be prescribed. In terms of the Dirichlet boundary conditions, the left ventricle is firstly fixed at the base, from moving in the vertical direction. During muscular contraction, the left ventricle experiences a degree of twist. In order to allow this torsional behaviour but still restrict the deformation to a level which is physiologically normal, a Dirichlet boundary condition is weakly imposed through application of an elastic boundary condition, with a prescribed stiffness k, around the epicardial base, as done in [25]. Lastly, in order to restrict motion in the xy axis, but still allow for torsional motion, zero displacement is enforced in the xy direction at the point of the apex of the left ventricle.

The Neumann boundary conditions are considered next. The inflow of blood into the ventricular cavity, during the diastolic filling stage of the cardiac cycle, imparts a hydrostatic pressure on the myocardial walls. To model this, an incremental surface pressure load is prescribed on the inner walls of the left ventricle. As specified in the work of Rama [25], and the citations therein, the surface pressure is assigned a value of 0 kPa and 1.5 kPa, at the start and end of diastolic filling, respectively. Due to blood not being able to seep out from the ventricles, it is assumed that the seepage flux for the entire domain of the left ventricle is zero.

5.2 Material parameters

With respect to cardiac modelling, a variety of parameters which influence the overall characteristics of the simulated model exist. Briefly noting, the parameters of concern include those associated with the strain energy function ψ^{S} during the diastolic filling stage, the active tension model during ejection, and the Windkessel model (see [26]). Incorporating the theory of porous media comes with an array of additional parameters linked to the various constituent phases and those needed to characterize the constitutive equations formulated for the seepage velocity and mass exchange function.

The rest fibre orientations θ_0 and rest sarcomere lengths l_0 of the epicardium are taken as -51° and 1.91μm, respectively. For the endocardium, these quantities are 66° and 1.78μm.

The input parameters relating to the solid tissue phase, and the fluid phases, which are contained within the blood saturating the solid skeleton, consists of the real densities $\rho_{0\alpha}^{\alpha R}$, and the reference volume fractions $n_{0\alpha}^{\alpha}$, when the left ventricle is in a state of rest. The parameters are given in Table (1)

Table 1. Prescribed TPM parameters associated with the constituents in the reference configuration, and the seepage velocity constitutive law.

Material parameter	Value	Unit	Source
Tissue density ρ_{0S}^{SR}	220	kg/m^3	[1, 27]
Blood density ρ_{0L}^{LR}, ρ_{0N}^{NR}	1060	kg/m^3	[28]
Solid r.v.f. n_{0S}^{S}	0.75	-	[29]
Liquid r.v.f. n_{0L}^{L}	0.1	-	-
Nutrient r.v.f. n_{0N}^{N}	0.15	-	-
Anisotropy parameter α_{F1}	0	-	[16]
Darcy permeability K^{F}	$2 \cdot 10^{-9}$	m^4/N$\cdot$s	[30]

In order to calibrate the passive and active material parameters, to the 2014 and 2016 patient-specific cardiac models, a comparison of the end diastolic volume (EDV) and end systolic volume (ESV) was performed. The EDV and ESV values were measured from experimental data accessed from the CMR scans. The measured EDV and ESV values for the 2014 and 2016 models may be viewed in Table (2).

Table 2. Experimental values for the EDV and ESV, in relation to the 2014 and 2016 models. [1]

Quantity	2014	2016	Unit
EDV	146	147	ml
ESV	72	80	ml

The calibrated passive and active material parameters may be viewed in [1, 22].

Calibration of the cardiac models has so far been conducted with the condition of $\hat{\rho}^{S}$=0. The adopted method for calibrating the growth model was proposed by Hopkins [1], whereby the 2014 scan is used as an initial starting point. With the addition of growth, this model is then calibrated against the EDV and ESV values of the 2016 model. The parameter which will be calibrated comprises solely of the maximum mass exchange rate $\hat{\rho}^{max}$. Growth function

parameters were used in accordance with Göktepe et al. [11], which were selected specifically to model a dilated heart. As such, the final calibrated value of $\hat{\rho}^{\max}$ was found to be $3.3 \cdot 10^{-5}\,\mathrm{kg/(mm^3 \cdot s)}$.

5.3 Analysis of the growth induced model

So far within this investigation, two model geometries have been simulated, corresponding to two different time periods, namely in the years of 2014 and 2016. The growth model discussed in the last section was implemented such that it would be able to predict the physiological changes that occurred between the interval, in terms of the mechanical and thermodynamic behaviour. This was done by calibrating the 2014 growth induced model ($\hat{\rho}^{\alpha} \neq 0$), to the 2016 ESV and EDV values. As stated, the 2016 CMR scans were taken after valve replacement surgery in 2015. While the EDV and ESV properties match those of left ventricle dilation characteristics, some do not. Therefore, further analysis of the 2016 data is too complex and lies outside the scope of this study. In addition, the triphasic growth model presented cannot distinguish between LVD conditions brought upon by valvular regurgitation, as this would involve a more in-depth study into the hemodynamic mechanics. As a starting point, the presented model is built to model a general case of LVD. This section will hence continue with a comparison of the initial state of the 2014 model, simulated with and without the inclusion of growth.

5.3.1 Analysis of the pressure-volume curves

After simulating the 2014 model with and without mass supply, over one heartbeat, the following results were produced, as shown by the pressure-volume curves in Fig.(3), and in Table (3).

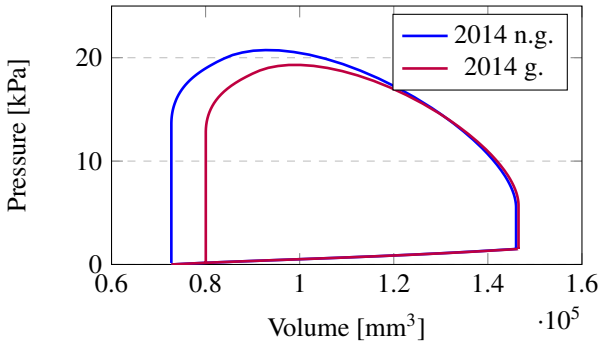

Figure 1. Pressure-volume curves of the 2014 model simulated with and without the inclusion of growth

From the data shown in the Table 3, it is apparent that deterioration in the condition of the heart is reflected by the growth model. The increase in EDV and ESV, with respect to the growth induced model, is an indication of the increase in volume which has occurred as a result of growth. In addition, the growth induced model appears to have reduced in peak pressure by 1.4 kPa, which denotes a reduced capacity. This result is analogous to the condition of LVD. The enlarged dilated left ventricle has an effect on the mechanical function, whereby weakening of the muscles is generally observed [31]. This deficiency may also be

Table 3. Cardiac results pertaining to the 2014 model, simulated with and without growth.

Parameter	2014 no growth	2014 growth induced	Unit
EDV	146	146.5	ml
ESV	72	80.0	ml
SV	74	66.5	ml
EDPVR gradient	28.0	26.4	Pa/ml
Peak pressure	20.8	19.4	kPa

noted by the reduction in SV, which correlates with the amount of blood ejected out the cavity into the various circulatory systems. Another feature which highlights the presence of LVD is the end diastolic pressure volume relationship EDPVR, given in terms of the slope at the point of EDV. In the case of LVD, the EDPVR gradient is generally observed to decrease, which signifies a decrease in vascular stiffness and hence a debilitation of the cardiac tissue [31]. This is in agreement to the results shown in Table (3), whereby the EDPVR is seen to reduce by 2.4 Pa/ml with the addition of growth. [31]

5.3.2 Changes in mechanical behaviour

Cardiac dilation results in mechanical and functional changes in the left ventricle. Understanding the abnormalities which occur may be found in analysing the stresses and strains that the cardiac tissue experiences during its activity. This section will comprise an observation of the fibre stresses and strains of the initial state of the left ventricle, simulated using the 2014 geometrical model with no mass supply, and compared against that using the growth induced model. For the purpose of illustrating this, the fibre stress and strain within the mid section of the ventricle, and along the outer surface of the epicardium, will be focused on. This data is shown in Fig.(2).

From the depiction of the pressure-volume curve in Fig.(1), which is represented quantitatively in Table (3), the growth induced model indicates that the ejection capacity had been compromised. It is expected that this reduction in mechanical load will coincide with the stresses and strains of the myocardium, which is confirmed through analysis of Fig.(2). From Fig.(2), it may be seen that during diastolic filling, at a point where minimal growth has developed (due to low states of stress), the fibre stress and strain of the two models, occur in tandem. However, as the stress, and hence the amount of growth increases due to stretching of the sarcomeres, the stress and strain of the growth induced model is seen to reduce below that of no-growth model. The pattern and values of the strains, shown in Fig.(2), is analogous to that presented in the work of Yu et al. [32], where a reduction of strains were documented in relation to an evaluation of left ventricular behaviour in patients with LVD.

In terms of the theory of porous media, the perfusion effects are greatly influenced by the mechanical action that the heart is subjected to. It may be understood that with a decrease in stress and strain, as a result of the inclusion of growth and remodelling, the pore pressure is expected to behave in a synchronous manner. This relationship may be viewed in the graph which denotes the evolution of the pore pressure against time over one cardiac cycle, as shown by Fig.(3). Commenting on the general characteristics of the pore pressure evolution of the two models, the pore pressure is observed to decrease during diastolic filling. This reduction may be attributed to the stretching of the muscle fibres, which would translate into expanded pore spaces. As the ejection phase is initiated, and the left ventricle contracts, the pore spaces

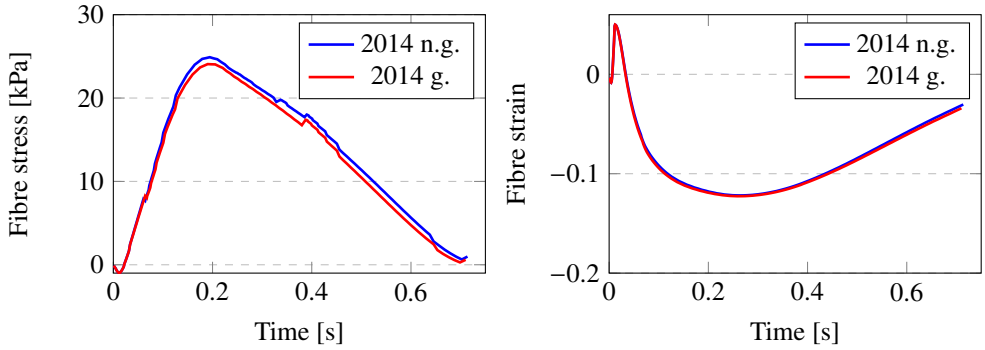

Figure 2. Fibre stress (left), and fibre strain (right), results generated from the growth induced and no-growth 2014 model.

would similarly shrink in size, which would therefore increase the pore pressure until the relaxation phase begins, whereby a stabilization of the pore pressure towards the initial state would then take place. The disturbance in the pore pressure distribution is a result which is inconclusive, and could however be a result of numerical instabilities.

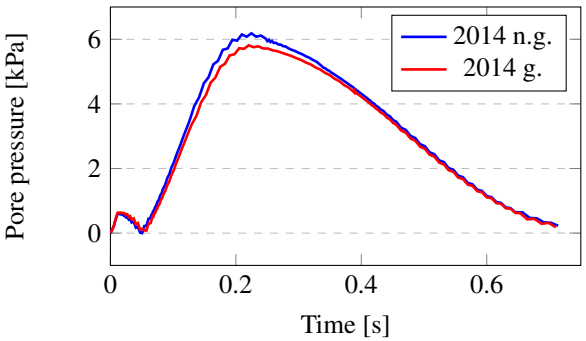

Figure 3. Pore pressure evolution, over a full cardiac cycle, which displays the relationship between the growth induced and no-growth 2014 model.

5.3.3 Changes in the volume fraction quantities

Predicting how the densities of the various constituents change within the heart in relation to growth proliferation is an important aspect. Degradation of the heart may correlate to abnormalities associated with a starvation of nutrients (such as oxygen supply)[7]. In addition, hypertrophy results in an increased solid tissue density, which results in a reduced relative blood tissue ratio [29, 33]. Consequently, a stiffening of the cardiac tissue and a reduction in nutrient provision may arise in these areas, which could lead to impaired ventricular function [7].

Fig.(4) illustrates the relationship between the sarcomere length, growth Jacobian J_g and the solid volume fraction n^S. For the case of LVD, a stretch induced growth function is employed. Hence, the degree of growth may be closely related to the sarcomere length,

which also then has influence in relation to n^S. This relation is apparent through observation of Fig.(4), whereby high values across all three parameters are viewed to occur at the top portion of the myocardium, in particular, at the end of diastolic filling. With eccentric growth, an elongation of the muscle fibres occurs due to a deposition of sarcomeres. Consequently, the deposition of sarcomeres results in an increased solid tissue mass.

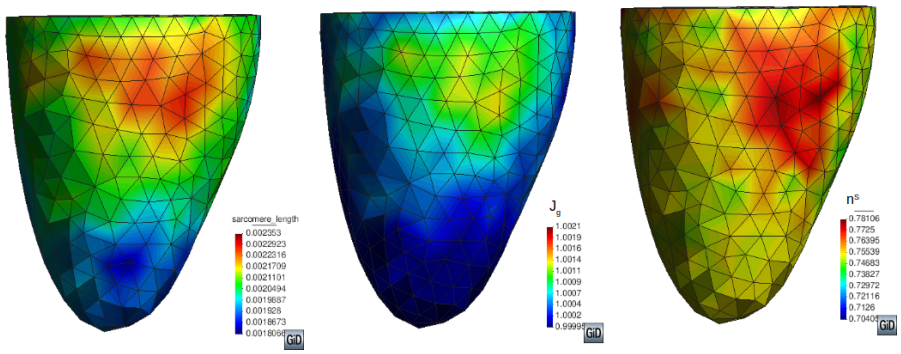

Figure 4. Illustration of the sarcomere length, growth Jacobian and solid volume fraction, at EDV.

To demonstrate the effect of the inclusion of growth on the solid and nutrient volume fractions, an evolution of these parameters over an entire cardiac cycle, measured at the point which displayed the greatest level of growth, was conducted and is presented graphically in Fig.(5). In addition, the point evolution of the growth Jacobian J_g, is shown in Fig.(6).

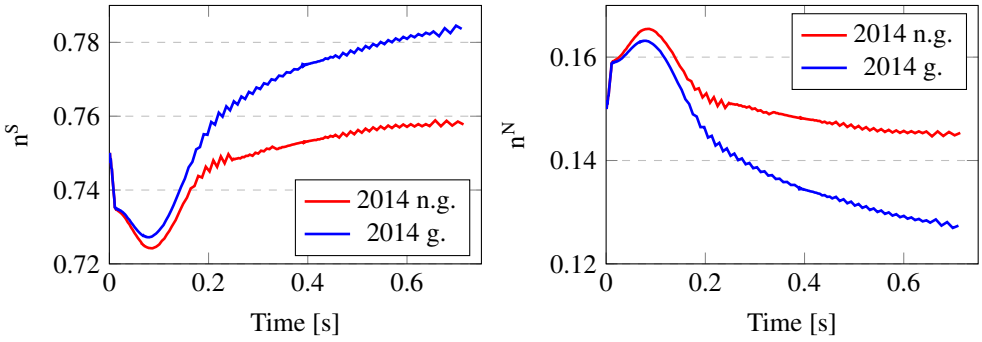

Figure 5. Evolution of the solid and nutrient volume fraction quantities, over a complete cardiac cycle, for the case of growth and no-growth.

From Fig.(5) and Fig.(6), it may be observed that with an increase in growth, an overall reduction in the blood tissue ratio occurs. During diastolic filling and early parts of the contraction stage, during which the amount of growth is still minimal, the blood tissue ratio is seen to increase. This feature is influenced by the mechanical loads exerted on the left ventricle within that phase of the cardiac cycle, whereby the left ventricle expands due to diastolic filling and an overall stretching of the muscle fibres occurs. The expansion of tissue would thus result in an increased pore space size, allowing the fluid to enter this region. A greater fluid density would therefore be incurred. As the pore spaces contract, the pore pressure would increase, causing the fluid to be expelled. This would hence result in an

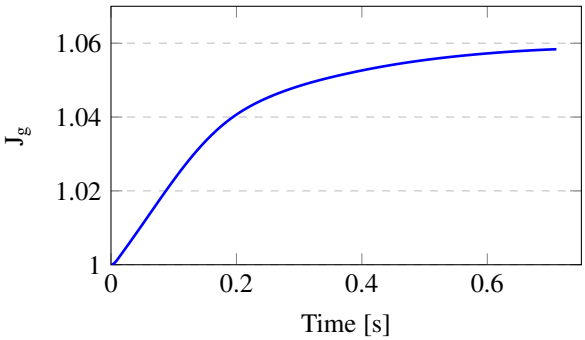

Figure 6. Progression of the growth Jacobian J_g, over a full cycle, at the point which displayed maximum growth.

increased relative tissue density. It may be observed however, that the increase in n^S is greater with respect to the growth induced model. This suggests that the tissue density is greatly influenced by the mass supply function. In addition, with the no-growth model, the volume fractions are observed to stabilize and approach the reference state ($n^{\alpha}_{0\alpha}$), once the heartbeat is complete. In contrast, with respect to the growth induced model, higher values of n^S are noted at the end of the heartbeat, compared to those at the beginning of the simulation, which signifies permanent tissue growth. This feature correlates well with the description of growth in relation to LVD.

Inclusion of the nutrient phase was motivated on the basis that more control over the depletion of the total fluid volume, as a result of growth, would be realised. This was done by coupling the mass supply function solely between the solid tissue phase and the nutrient phase. As such, during simulation of the growth induced model, it is expected that the liquid volume will be consumed less compared to the nutrient quantity. Table (4) displays the final volume fraction values, obtained at the end of the simulation, between the growth induced and no-growth models.

Table 4. Volume fraction values at the end of the cardiac cycle, using the no-growth and growth TPM models. Changes in the volume fraction quantities and the percent contribution of the fluid phases towards the solid volume are also presented

Parameter	n^S	n^N	n^L
No-growth model v.f.	0.758	0.146	0.096
Growth model v.f.	0.784	0.127	0.089
Change in v.f.	0.026	-0.019	-0.007
% fluid contribution	-	73%	27%

From Table (4), it may be observed that the contribution towards growth of the tissue phase, is greater with respect to the nutrient phase as compared to the liquid phase. This result agrees with the expected assumption that the nutrient phase will deplete more during growth. However, the reason that n^L decreases with growth may be found from the mathematical formulation of the mass supply terms shown in the field equations. A solution to making the growth fully dependent on the solid and nutrient volume fractions may lie in adapting

the balance equations, and the term containing the mass supply function specifically. By replacing the respective real density $\rho^{\alpha R}$, shown in the final term of Eq.$(6)_1$ and Eq.$(6)_3$, with a scalar factor, the mass supplied would be fully coupled between the nutrient and solid phase. In this regard, it is hypothesised that the liquid phase would not be affected by growth.

6 Conclusions

This section will highlight the conclusions drawn in relation to the implementation of the triphasic TPM model, and its application to the example of a patient specific left ventricle model.

This research consisted of implementing a triphasic framework, based on the Theory of Porous Media. This was firstly achieved by extending the current biphasic model present within the in-house built solid mechanics software SESKA. An additional degree of freedom was included, in the form of a nutrient volume fraction, which allowed for mass exchange in context of growth and remodelling proliferation. Mass supply was induced through a stretch driven growth function and was implemented using an adapted method developed by Werner [18]. Furthermore, the triphasic model was coupled with cardiac mechanics framework in SESKA, and was hence used to simulate patient specific models in relation to RHD. This study was however limited to using the 2014 CMR scans, as the 2016 scans were taken after the patient was admitted for valve replacement. This rendered the analysis of the 2016 scans, as outside the scope of this study. In addition, the model presented could only describe the general case of LVD, and not that caused by different valvular regurgitation conditions. This could however be investigated further and incorporated into the triphasic model in future work.

The results produced by the 2014 model, simulated with growth, matched up closely to those expected in dilated left ventricles. This was seen by the increase in ESV and EDV results, which indicated an increase in cavity volume in states of rest and at maximum capacity, respectively. In addition, reductions in the SV, peak pressure, and the EDPVR gradient, were observed in the 2014 growth model, which conveyed a reduced pumping capacity and weakening of the heart tissue, and are typical characteristics related to LVD. Reductions in pore pressures, and fibre stresses and strains were additionally noted. This correlated with observations documented in the work of Yu et al. [32]. As such, it may hence be concluded that the triphasic growth induced model may be sufficiently used to model hearts associated with LVD.

One of the key objectives of this research was to implement the third phase, such that it would contribute to the mass exchange process and would therefore control the volume levels of the liquid constituent. It was found that with growth, a slight reduction in n^L occurred, which was found to stem from the mathematical construct of the balance equations. However, the reduction in n^L was observed to be minimal in comparison to the reduction in n^N. Hence, the overall objective was still satisfied.

Acknowledgement

This research has been supported by the National Research Foundation (NRF) of South Africa (Grant Nos. 104839 and 105858). Opinions expressed and conclusions arrived at are those of the author and are not necessarily to be attributed to the NRF.

References

[1] G. Hopkins, *Growth, Modelling and Remodelling of Cardiac Tissue: A Multiphase Approach* (University of Cape Town, 2017)

[2] W. Rosamond, K. Flegal, G. Friday, K. Furie, A. Go, K. Greenlund, N. Haase, M. Ho, V. Howard, B. Kissela et al., Circulation **115**, e69 (2007)

[3] D.P. Zipes, P. Libby, R.O. Bonow, D.L. Mann, G.F. Tomaselli, *Braunwald's Heart Disease: A Textbook of Cardiovascular Medicine* (Elsevier Health Sciences, 2018)

[4] H.D. Allen, D.J. Driscoll, R.E. Shaddy, T.F. Feltes, *Moss & Adams' Heart Disease in Infants, Children, and Adolescents: Including the Fetus and Young Adult* (Lippincott Williams & Wilkins, 2013)

[5] E. Marijon, M. Mirabel, D.S. Celermajer, X. Jouven, The Lancet **379**, 953 (2012)

[6] J.E. Hall, *Guyton and Hall textbook of medical physiology* (Saunders, 2015)

[7] A. Katz, *Physiology of the Heart, Fifth Edition* (Wolters Kluwer Health/Lippincott Williams & Wilkins Health, 2010)

[8] L.H. Opie, P.J. Commerford, B.J. Gersh, M.A. Pfeffer, The Lancet **367**, 356 (2006)

[9] G. Himpel, E. Kuhl, A. Menzel, P. Steinmann, Computer Modeling in Engineering and Sciences **8**, 119 (2005)

[10] E. Kuhl, R. Maas, G. Himpel, A. Menzel, Biomechanics and modeling in mechanobiology **6**, 321 (2007)

[11] S. Göktepe, O.J. Abilez, E. Kuhl, Journal of the Mechanics and Physics of Solids **58**, 1661 (2010)

[12] R.C.P. Kerckhoffs, J.H. Omens, A.D. Mcculloch, Mechanics Research Communications **42**, 40 (2011)

[13] S. Göktepe, O.J. Abilez, K.K. Parker, E. Kuhl, Journal of Theoretical Biology **265**, 433 (2010)

[14] M.K. Rausch, A. Dam, S. Göktepe, O.J. Abilez, E. Kuhl, Biomech Model Mechanobiol **10**, 799 (2011)

[15] D. Werner, T. Ricken, A. Ferreira Pfeiffer, Proceedings in Applied Mathematics and Mechanics **13**, 63 (2013)

[16] T. Ricken, J. Bluhm, Archive of Applied Mechanics **80**, 453 (2010)

[17] T. Ricken, A. Schwarz, J. Bluhm, Computational Materials Science **39**, 124 (2007)

[18] D. Werner, *Two Scale Multi-component and Multi-phase Model for the Numerical Simulation of Biological Growth Processes in Saturated Porous Media - at the Example of Fatty Liver in Human* (Technical University of Dortmund, 2017)

[19] W. Ehlers, J. Bluhm, *Porous media: theory, experiments and numerical applications* (Springer Science & Business Media, 2013)

[20] A. Menzel, E. Kuhl, Mechanics Research Communications **42**, 1 (2012)

[21] E. Kuhl, Journal of the Mechanical Behavior of Biomedical Materials **29**, 529 (2014)

[22] A. Mosam, *A tri-phasic continuum model for the numerical analysis of biological tissue proliferation using the Theory of Porous Media. Application to cardiac remodelling in rheumatic heart disease* (University of Cape Town, 2019)

[23] G. Eipper, *Theorie und Numerik finiter elastischer Deformationen in fluidgesättigten porösen Festkörpern* (Inst. für Mechanik (Bauwesen), 1998)

[24] W. Ehlers, N. Karajan, B. Markert, A. Acartürk, Proceedings in Applied Mathematics and Mechanics **5**, 27 (2005)

[25] R. Rama, *Proper Orthogonal Decomposition with Interpolation-based Real-time Modelling of the Heart* (University of Cape Town, 2017)

[26] M.A. Essack, *Material Parameter Identification for Modelling the Left Ventricle in the Healthy State* (University of Cape Town, 2014)

[27] K.C. Vinnakota, AJP: Heart and Circulatory Physiology **286**, H1742 (2004)

[28] J. Cutnell, K. Johnson, D. Young, S. Stadler, *Physics, 10th Edition* (Wiley, 2015)

[29] A. Indermühle, R. Vogel, P. Meier, S. Wirth, R. Stoop, M.G. Mohaupt, C. Seiler, European Heart Journal **27**, 1571 (2006)

[30] W.A. Wall, L. Wiechert, A. Comerford, S. Rausch, International Journal for Numerical Methods in Biomedical Engineering **26**, 807 (2010)

[31] R. Klabunde, *Cardiovascular Physiology Concepts, Second Edition* (Wolters Kluwer Health/Lippincott Williams & Wilkins, 2011)

[32] Y. Yu, S. Yu, X. Tang, H. Ren, S. Li, Q. Zou, F. Xiong, T. Zheng, L. Gong, Journal of International Medical Research **45**, 2092 (2017)

[33] J.P. Cleutjens, W.M. Blankesteijn, M.J. Daemen, J.F. Smits, Cardiovascular Research **44**, 232 (1999)